Journal of Zhejiang University-SCIENCE A (Applied Physics & Engineering)
ISSN 1673-565X (Print); ISSN 1862-1775 (Online)
www.jzus.zju.edu.cn; www.springerlink.com
E-mail: jzus@zju.edu.cn

Time-domain model for wheel-rail noise analysis at high operation speed*

Jian HAN[1], Shuo-qiao ZHONG[1], Xin ZHOU[1], Xin-biao XIAO[1], Guo-tang ZHAO[1,2], Xue-song JIN[†‡1]

([1]*State Key Laboratory of Traction Power, Southwest Jiaotong University, Chengdu 610031, China*)

([2]*China Railway Corporation, Beijing 100844, China*)

[†]E-mail: xsjin@home.swjtu.edu.cn

Received Oct. 21, 2016; Revision accepted Mar. 5, 2017; Crosschecked July 12, 2017

Abstract: This paper develops a numerical model for wheel-rail noise analysis in the time-domain. This model for wheel-rail noise is based on vehicle-track coupling dynamics considering the effect of flexible wheelsets and track, and a transient wheel-rail noise prediction method. This model can approximatively characterize the components of vibration and noise in the frequency range up to 3.5 kHz. The wheel-rail forces are calculated and shown in both time and frequency domains by using the vehicle-track coupling dynamic model. Then the vibration and sound of the flexible wheelset are calculated by the transient finite element-boundary element (FE-BE) prediction model at 300 km/h, in which the effects of random irregularity and discrete supporting excitation are considered. The numerical results calculated by using the present model are discussed. The present model is also used to calculate the effect of corrugation with wavelengths of 40 mm to 300 mm on wheel-rail noise. The numerical results can be useful for academic research and engineering application to railway noise and vibration.

Key words: Vibration and sound; Wheel-rail; Vehicle-track coupling dynamics; Rigid wheelset; Flexible wheelset; High-speed operation

http://dx.doi.org/10.1631/jzus.A1600692 **CLC number:** TB533.2

1 Introduction

For high-speed railway lines with curves of large radii, curve squeal noise can be effectively controlled. It is wheel-rail rolling noise that is one of the main noise sources in high-speed operation (Jin, 2014). The study of the wheel-rail rolling noise mechanism began in the early 1970s. Remington (1987; 1988) is one of the earlier scholars on wheel-rail rolling noise. Based on the dynamic interaction of the wheel-rail system, he set out the mechanism of wheel-rail rolling noise, and put forward the earliest wheel-rail rolling noise prediction model. Thompson (1993a; 1993b; 1993c; 1993d; 1993e) further developed and perfected the wheel-rail rolling noise model on the basis of Remington (1987; 1988)'s research. Then the European Railway Institute (ERRI) developed the track-wheel interaction noise software (TWINS) on the basis of Thompson (2009)'s improved wheel-rail noise prediction model. A large number of field verifications showed that TWINS predicted wheel-rail rolling noise in the frequency-domain accurately and reliably at running speeds of 60–150 km/h (Thompson *et al*., 1996). The model also has a high computing speed. In using TWINS, wheel-rail dynamic characteristics are predicted by using a 2D axisymmetric model. The model considers the vibration at only seven points (one point on the rim, five points on

‡ Corresponding author

* Project supported by the National Natural Science Foundation of China (Nos. U1434201 and 51475390), the National Key Technology R&D Program of China (Nos. 2016YFB1200503-02 and 2016YFB1200506-08), and the 2015 Doctoral Innovation Funds of Southwest Jiaotong University, China

ORCID: Jian HAN, http://orcid.org/0000-0002-7891-7164

the web, and one point on the hub) on the cross-section of a wheel, which does not fully reflect vibration characteristics of the whole wheel structure, especially in the high frequency range. In addition, it is difficult to predict the vibration of wheels with complex cross-sections by using TWINS. On the basis of TWINS, a 3D finite element model of wheel and track has been developed to study vibration and sound radiation (Ma, 2007; Fang *et al*., 2011). However, wheel-rail contact in these simulations also adopts a linear Hertz contact in the frequency domain, which is not suitable for reflecting the nonlinear features of transient high-speed wheel-rail interactions, especially when the wheel-rail surfaces have partial deflects. In such a situation, the mechanism of wheel-rail noise is very complex (Delavaud *et al*., 2010). Wu and Thompson (2002) considered nonlinear wheel-rail interaction in simulating wheel-rail noise by adopting the combination of time-domain and frequency-domain methods. However, in the time-domain model, wheelsets are simplified as rigid structures to calculate wheel-rail force, which cannot reflect their high frequency characteristics. The applicable frequency range of the existing time-domain models for predicting wheel-rail noise is less than 2 kHz (Thompson, 2009). One limitation is due to the Timoshenko beam model which is a suitable approach only up to 2 kHz. The other important limitation is due to the assumption of a rigid wheel that is also only appropriate for low frequencies. The contribution of the wheel in wheel-rail noise is dominant above 2 kHz (Thompson, 2009). Considering wheelset flexibility in the time domain for calculating wheel-rail noise is therefore important. In recent research, wheelset flexibility has begun to be considered in vehicle dynamics and analysis of its vibration to cover the audible frequencies is being carried out.

In this study, the time-domain model for wheel-rail noise is developed based on vehicle-track coupling dynamics and the transient wheel-rail noise prediction method. In the present model, non-linear wheel-rail contact and wheelset flexibility are both considered. The model computes wheel-rail noise above 2 kHz by considering wheel flexibility. It is assumed that the analysis frequency of wheel-rail force over 2 kHz can ignore the influence of the rail. Then the vibration and sound of the wheelset and track are calculated by using a transient finite element-boundary element (FE-BE) prediction model. Finally, an extension of the time-domain model is discussed with a discussion of the effect of corrugation on wheel-rail noise.

2 Rigid-flexible coupling dynamic model of vehicle and track

A dynamic model of a high-speed railway vehicle coupled with a track has been developed based on the conventional dynamic theory (Zhai, 1996; Jin and Wen, 2008). Here, the car body and the frames of the two bogies are still modeled as rigid bodies, but the wheelsets are modeled as flexible structures, as shown in Fig. 1. The primary and secondary suspension systems of the vehicle are modeled with spring-damper elements. A triple-layer flexible model of discrete elastic support is adopted to simulate the slab track (Han *et al*., 2015). In the new vehicle-track coupling dynamic model, flexible wheelsets and the flexible track are considered so as to obtain wheel-rail forces containing the components of frequency up to 3.5 kHz which covers the main frequencies contributing to wheel-rail noise.

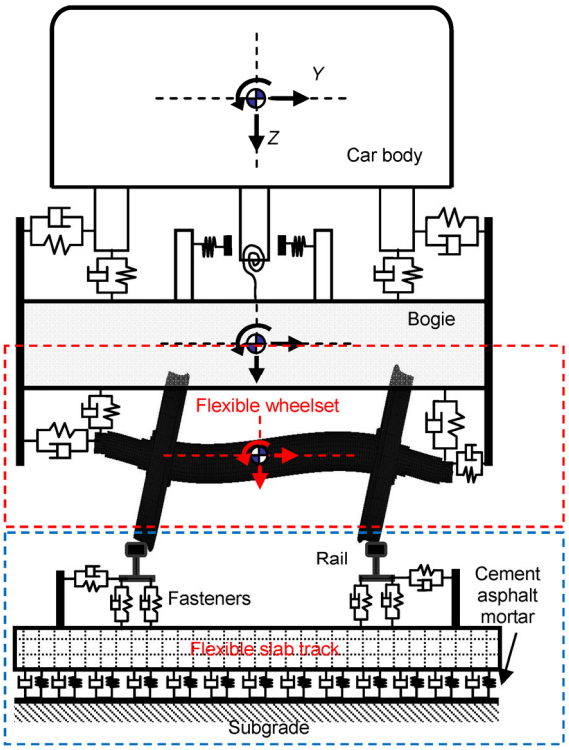

Fig. 1 Vehicle-track rigid-flexible coupling dynamic model

2.1 Dynamic model of flexible wheelsets

Many studies have been conducted on flexible wheelset modeling (Chaar, 2007). The existing models of a flexible wheelset can be categorized as lumped mass models (Popp *et al*., 1999), continuous wheelset axle models (Szolc, 1998a; 1998b), wheel-web-as-membrane models (Popp *et al*., 2003), and finite-element wheelset models (Meinders, 1998; Baeza *et al*., 2011). A detailed wheel-rail contact relationship is discussed to consider the effect of a flexible wheelset. The influence of wheelset flexibility and the gyroscopic effect on the motion of the contact point is considered. The 'online searching' for wheel-rail contact points is developed (Zhong *et al*., 2014; 2015; 2016).

The wheelset eigenmodes and natural frequencies are calculated using a 3D finite element model of the wheelset implemented in ANSYS. The diameter of the wheel is 0.86 m. This paper assumes that equipment attached to the axle, such as the brake disc and the gearbox, is not included in the wheelset model. The present work focuses on all modes below 3.5 kHz (Fig. 2), which include axle bending modes, axle expansion and shrinkage modes, axle rotation modes, wheel modes in-plane, wheel modes out-of-plane, and the combinations of those modes.

Based on 3D solid dynamics finite element theory, the *i*th (*i* is the position of each wheelset) wheelset differential motion equation at the moment *t* can be written as

$$\boldsymbol{M}_i\ddot{\boldsymbol{u}}_i(t)+\boldsymbol{K}_i\boldsymbol{u}_i(t)=\boldsymbol{F}_i(t),\ i=1,2,3,4, \tag{1}$$

where $\ddot{\boldsymbol{u}}_i(t)$ and $\boldsymbol{u}_i(t)$ are the acceleration and displacement vectors, respectively. $\boldsymbol{M}_i$ and $\boldsymbol{K}_i$ are the mass and stiffness matrices, respectively. $\boldsymbol{F}_i(t)$ is the external force vector, which can be written as

$$\boldsymbol{F}_i(t)=\boldsymbol{F}_{xi}(t)+\boldsymbol{F}_{yi}(t)+\boldsymbol{F}_{zi}(t), \tag{2}$$

where the subscripts x, y, and z indicate the total force components in the three directions. Two main force systems acting on the wheelset are related to the primary suspension systems and the wheel-rail contact points. So the three force component vectors can be written as

$$\boldsymbol{F}_{xi}(t)=\left(\boldsymbol{F}_{\mathrm{fL}xi}+\boldsymbol{F}_{\mathrm{fR}xi}\right)+\left(\boldsymbol{F}_{\mathrm{CL}xi}+\boldsymbol{F}_{\mathrm{CR}xi}\right), \tag{3}$$

$$\boldsymbol{F}_{yi}(t)=\left(\boldsymbol{F}_{\mathrm{fL}yi}+\boldsymbol{F}_{\mathrm{fR}yi}\right)+\left(\boldsymbol{F}_{\mathrm{CL}yi}+\boldsymbol{F}_{\mathrm{CR}yi}\right), \tag{4}$$

$$\boldsymbol{F}_{zi}(t)=\left(\boldsymbol{F}_{\mathrm{fL}zi}+\boldsymbol{F}_{\mathrm{fR}zi}\right)+\left(\boldsymbol{F}_{\mathrm{CL}zi}+\boldsymbol{F}_{\mathrm{CR}zi}\right), \tag{5}$$

where $\boldsymbol{F}_{\mathrm{fL}xi}$ and $\boldsymbol{F}_{\mathrm{fR}xi}$ are the longitudinal components of the left and right primary suspension force vectors, respectively. $\boldsymbol{F}_{\mathrm{CL}xi}$ and $\boldsymbol{F}_{\mathrm{CR}xi}$ are the longitudinal components of the left and right wheel-rail contact force vectors, respectively. $\boldsymbol{F}_{\mathrm{fL}yi}$ and $\boldsymbol{F}_{\mathrm{fR}yi}$ are the lateral components of the left and right primary suspension force vectors, respectively. $\boldsymbol{F}_{\mathrm{CL}yi}$ and $\boldsymbol{F}_{\mathrm{CR}yi}$ are the lateral components of the left and right wheel-rail contact force vectors, respectively. $\boldsymbol{F}_{\mathrm{fL}zi}$ and $\boldsymbol{F}_{\mathrm{fR}zi}$ are the vertical components of the left and right primary suspension force vectors, respectively. $\boldsymbol{F}_{\mathrm{CL}zi}$ and $\boldsymbol{F}_{\mathrm{CR}zi}$ are the vertical components of the left and right wheel-rail contact force vectors, respectively.

Eq. (1) is solved by the modal superposition method, then $\boldsymbol{u}_i(t)$ can be written as

$$\begin{aligned}\boldsymbol{u}_i(t)=&\boldsymbol{\varphi}_{i1}q_{i1}(t)+\boldsymbol{\varphi}_{i2}q_{i2}(t)+\cdots+\boldsymbol{\varphi}_{ik}q_{ik}(t)\\&+\cdots+\boldsymbol{\varphi}_{iN}q_{iN}(t)=\boldsymbol{\Phi}_i\boldsymbol{q}_{ik}(t),\end{aligned} \tag{6}$$

where N is the total number of modes considered. The subscript k indicates the kth mode. $\boldsymbol{q}$ is the normal modal coordinate vector. $\boldsymbol{\Phi}$ is the eigenvalue matrix which consists of the column modal vectors $\boldsymbol{\varphi}_{ik}$. Then the first and the second derivatives of $\boldsymbol{u}_i(t)$ can be written as

$$\dot{\boldsymbol{u}}_i(t)=\boldsymbol{\Phi}_i\dot{\boldsymbol{q}}_{ik}(t),\ \ddot{\boldsymbol{u}}_i(t)=\boldsymbol{\Phi}_i\ddot{\boldsymbol{q}}_{ik}(t). \tag{7}$$

Substituting Eqs. (6) and (7) into Eq. (1), the motion equation can be written as

$$\boldsymbol{M}_i\boldsymbol{\Phi}_i\ddot{\boldsymbol{q}}_{ik}(t)+\boldsymbol{K}_i\boldsymbol{\Phi}_i\boldsymbol{q}_{ik}(t)=\boldsymbol{F}_i(t). \tag{8}$$

According to orthogonalization theory, the mass and stiffness matrices are diagonalized. Then the motion equation can be decoupled as

$$\ddot{\boldsymbol{q}}_{ik}(t)+\omega_k^2\boldsymbol{q}_{ik}(t)=\boldsymbol{\varphi}_{ik}^{\mathrm{T}}\boldsymbol{F}_i(t), \tag{9}$$

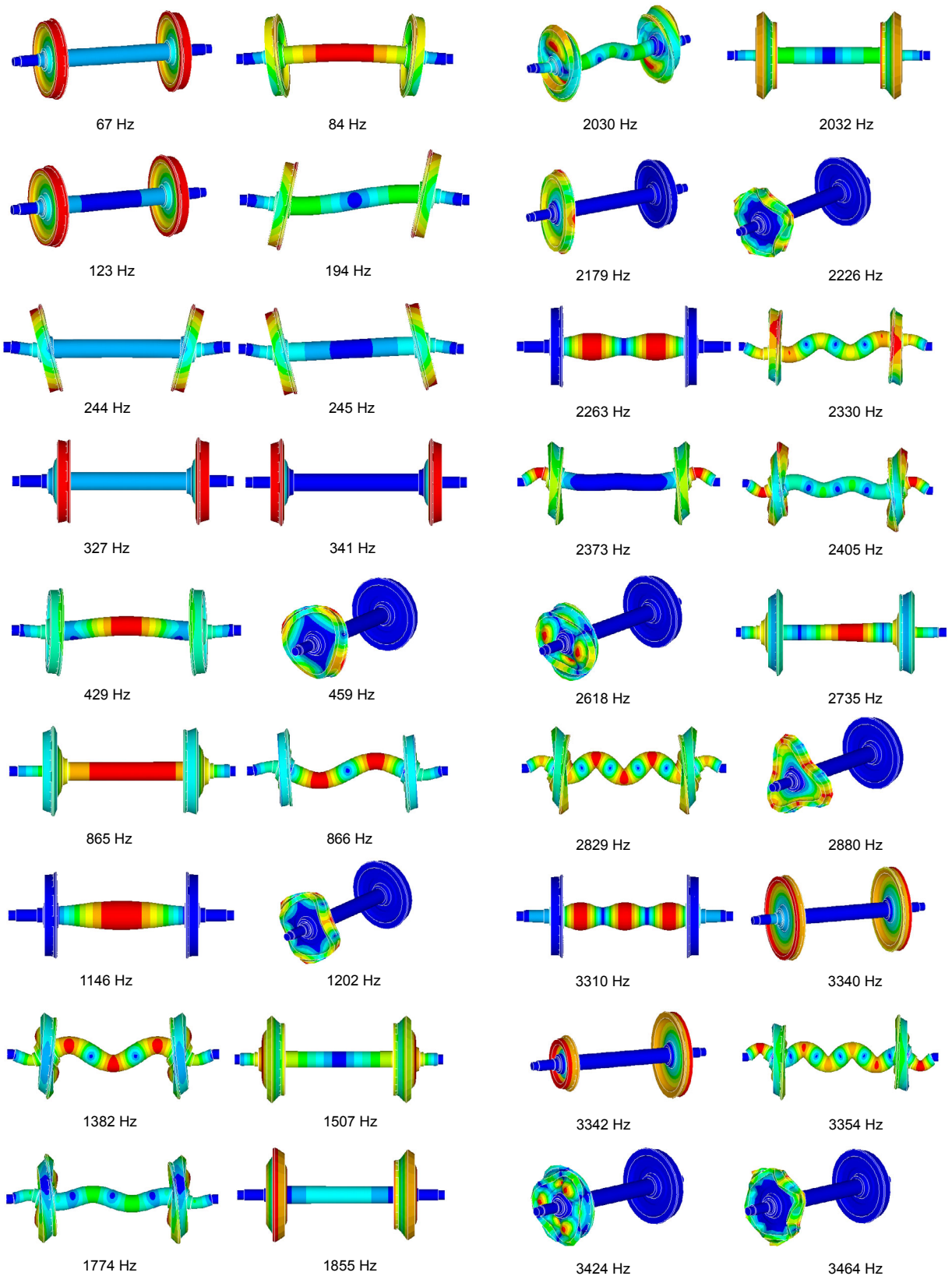

Fig. 2 Mode shapes of high-speed wheelset below 3.5 kHz

where the second derivative of $\boldsymbol{q}_{ik}$ at each time step can be solved by the explicit integral algorithm. ω_k is the natural frequency of the wheelset. Then Eqs. (6) and (7) can be used to calculate the nodal displacement, velocity, and acceleration.

This flexible wheelset model can consider the combining influence of the wheelset axle deformations in the two planes which are respectively, parallel and vertical to the track level plane. The model can also consider the deformation of the tread and web of the wheel.

2.2 Dynamic model of flexible track

The dynamic model of slab track considers rails, fastener systems, slabs, and subgrade (Fig. 1). The rail is treated as a Timoshenko beam resting on rail pads, and the lateral, vertical, and torsional motions of the rail are simultaneously taken into account (Xiao *et al.*, 2008). The length of rail is 62.5 m in the track window. The mode number of the rail is 300, and the highest mode frequency is 2 kHz. The vertical and lateral rail supporting stiffnesses are 40 kN/mm and 20 kN/mm, respectively. The slabs are modeled using the 3D finite element method (Han *et al*., 2015; Ling *et al*., 2015). The rail fastener systems and subgrade are modeled using periodic discrete viscoelastic units. The finite element model of the slab (CRTS II) has 5538 solid elements and 23 328 degree of freedoms (DOFs). The length of one slab is 6.25 m. The geometric dimensions of its cross-section are 2.55 m×0.2 m. The vibration of the slab can be easily described in a second-order differential equation in terms of generalized coordinates, as expressed by Eq. (10). Modal analysis of the slab is carried out by means of ANSYS to obtain 20 order modes, by using which Eq. (10) is decoupled and solved according to the modal superposition principle.

$$\boldsymbol{M}_{si}\ddot{\boldsymbol{u}}_{si}+\boldsymbol{C}_{si}\dot{\boldsymbol{u}}_{si}+\boldsymbol{K}_{si}\boldsymbol{u}_{si}=\boldsymbol{F}_{rsi}+\boldsymbol{F}_{ssi}, \tag{10}$$

where $\boldsymbol{M}_{si}$, $\boldsymbol{C}_{si}$, and $\boldsymbol{K}_{si}$ are the mass, damping, and stiffness matrices, respectively, of the ith slab. $\ddot{\boldsymbol{u}}_{si}$, $\dot{\boldsymbol{u}}_{si}$, and $\boldsymbol{u}_{si}$ are the acceleration vector, velocity vector, and displacement vector of the ith slab, respectively. $\boldsymbol{F}_{rsi}$ is the load vector between the rail and the ith slab, and $\boldsymbol{F}_{ssi}$ is the load vector under the ith slab.

2.3 Dynamic model of wheel-rail interaction

Wheel-rail dynamic interaction modeling is the key to the vehicle-track coupling dynamic model. The calculation of wheel-rail contact forces includes a normal model and a tangent model. The normal model (Jin and Wen, 2008; Xiao *et al.*, 2014), which characterizes the relationship law of a normal load and deformation between the wheel and rail, is described by a nonlinear Hertzian contact spring with a unilateral restraint:

$$N(t)=\begin{cases}\left[\dfrac{1}{G_{\mathrm{Hertz}}}Z_{\mathrm{wrnc}}(t)\right]^{3/2}, & Z_{\mathrm{wrnc}}(t)>0,\\ 0, & Z_{\mathrm{wrnc}}(t)\le 0,\end{cases} \tag{11}$$

where G_{Hertz} is the wheel-rail contact constant ($\mathrm{m/N^{2/3}}$), which can be obtained using the Hertz contact theory. $Z_{\mathrm{wrnc}}(t)$ is the normal amount of compression at the wheel-rail contact point. $Z_{\mathrm{wrnc}}(t)$ is strictly defined as an approach between two distant points, one belonging to the wheel, and the other belonging to the rail. The wheel and the rail are assumed to be two elastic half-spaces. This approach is confined to the normal direction at the contact point of the wheel and the rail. $Z_{\mathrm{wrnc}}(t)>0$ indicates the wheel-rail in contact, and $Z_{\mathrm{wrnc}}(t)\le 0$ indicates their separation.

The tangential wheel-rail creep forces are calculated using the Shen-Hedrick-Elkins non-linear theory (Shen *et al.*, 1983). In this paper, when calculating the dynamic response of the vehicle-track, the tracing-curve-method (Chen and Zhai, 2004) is adopted to locate the wheel-rail spatial contact geometry. This can greatly reduce the computational time.

In this paper, the traction and braking effects on the longitudinal wheel-rail force are not considered because this paper focuses on wheel-rail rolling noise on a straight track at a constant speed. However, it is also very important to consider traction and braking forces in the processes of vehicle deceleration and acceleration and the longitudinal wheel-rail force also has effects on the lateral dynamics of the vehicle (Handoko and Dhanasekar, 2006; Zhang and Dhanasekar, 2012).

3 Model for wheel-rail vibration and sound

A 3D finite element model of the wheelset and track has been developed (Fig. 3). In the model, the normal forces ($F_{NR}(t)$, $F_{NL}(t)$ and $F'_{NR}(t)$, $F'_{NL}(t)$) and lateral creep forces ($F_{CR}(t)$, $F_{CL}(t)$ and $F'_{CR}(t)$, $F'_{CL}(t)$) obtained by the rigid-flexible coupling dynamic model of vehicle and track in Section 2 are added to the wheelset tread and the rail head. The acceleration of wheelset and track is solved by a direct integral method.

Then the vibration of the wheelset and track in the time domain is taken as the transient input of a boundary element method (BEM) acoustic model developed in the Virtual.Lab-Acoustic software to calculate the sound radiation of the wheelset and the rail. In the boundary element (BE) model, the BE grid of wheelset and track needs to be developed first. Then the vibration of wheelset and track surface is mapped to the BE grid. The sound pressures of the BE grid surface and any point in the spatial sound field are solved by the transient direct BEM. Sound radiation only considers wheelset, rail, and slab surface.

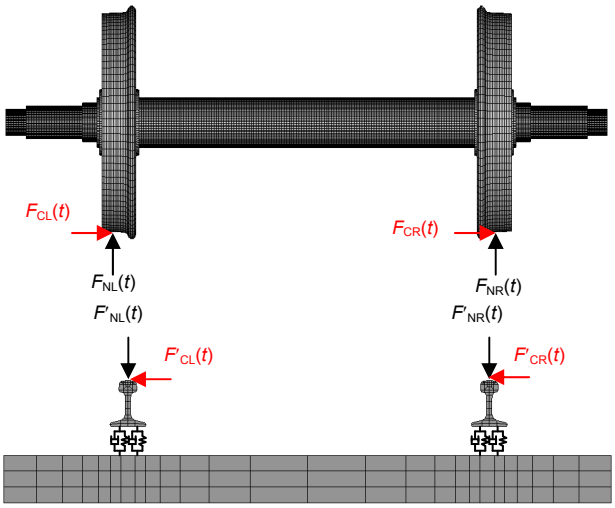

Fig. 3 Wheel-rail vibration model

4 Simulation results and discussion

4.1 Effect of flexible wheelsets on wheel-rail forces

Table 1 shows the effect of the wheelset flexibility on wheel-rail forces in the range lower than 3.5 kHz. In these cases, the other wheel-rail irregularities are not considered. Wheel-rail contact forces are mainly affected by the discrete support of sleepers generating a periodical excitation of about 133 Hz (the sleeper pitch is 0.65 m). The operating speed is 300 km/h. In Table 1, the symbol '+' indicates that the maximum of the wheel-rail normal force considering a flexible wheelset is larger than that of a rigid wheelset. The symbol '−' indicates that the maximum of the wheel-rail normal force considering a flexible wheelset is smaller than that of rigid wheelset. The symbol '0' indicates that the wheel-rail normal force of a flexible wheelset is equal to that of a rigid wheelset. Wheelset flexibility can lead to high-frequency fluctuations of the wheel-rail contact force (Baeza *et al*., 2008). The wheelset flexibility can lead to the wheel-rail contact force being smaller when the excitation frequencies are close to the natural frequencies, and being larger when the excitation frequencies are close to the anti-resonant frequencies.

Table 1 Effect of flexible wheelset on wheel-rail forces

Frequency (Hz)	Effect	Frequency (Hz)	Effect
123	0	2032	0
194	0	2179	−
244	−	2226	+
245	0	2263	0
327	0	2330	+
341	0	2373	0
429	−	2405	0
459	0	2618	0
865	0	2735	+
866	0	2829	0
1146	+	2880	−
1202	0	3310	0
1382	0	3340	0
1507	0	3342	0
1774	+	3354	+
1855	0	3424	0
2030	+	3464	0

Fig. 4 shows the wheel-rail normal force corresponding to rigid wheelset and flexible wheelset below 3.5 kHz. The rail surface irregularity is random with wavelengths of 0.02–10 m. The amplitude of this random irregularity is 0.02 mm. The speed of the high-speed vehicle is 300 km/h. f_s is the frequency due to discrete sleepers.

Fig. 4a shows that the wheel-rail contact forces considering wheelset flexibility are similar to those

for wheelsets that are rigid in the time domain. Fig. 4b is obtained by Fourier transform of Fig. 4a. Fig. 4b shows that the main difference occurs at high frequency.

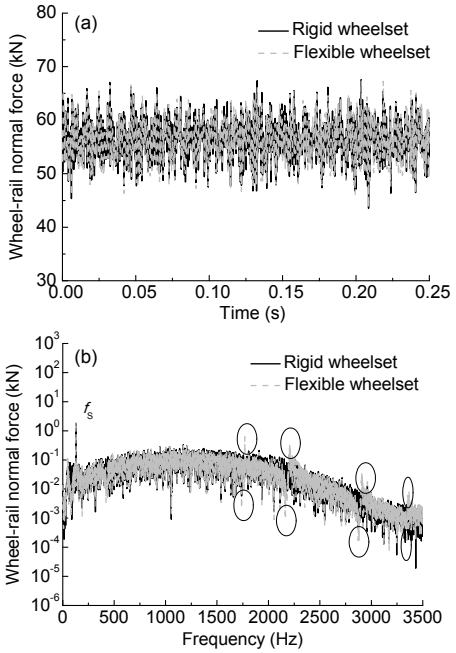

Fig. 4 Wheel-rail normal forces of rigid wheelset and flexible wheelset (below 3.5 kHz)
(a) Time domain; (b) Frequency domain

The wheel-rail contact forces considering wheelset flexibility are lower when wavelength roughness excites a natural frequency of the wheelset, and higher when wavelength roughness excites an anti-resonance frequency. Wheel-rail contact force fluctuates in high frequency due to wheelset flexibility and wheel-rail nonlinear contact relationship.

4.2 Effect of flexible wheelset on vibration and sound

Fig. 5 shows the acceleration on the nominal rolling contact point in the vertical direction in the time domain and frequency domain under random irregularity excitation.

Fig. 5a indicates that the acceleration level of a flexible wheelset is slightly larger than that of a rigid wheelset in the time domain. Fig. 5b shows that the acceleration of a flexible wheelset is similar to that of a rigid wheelset below 500 Hz. The accelerations of flexible wheelsets at higher frequency have more peaks and valleys.

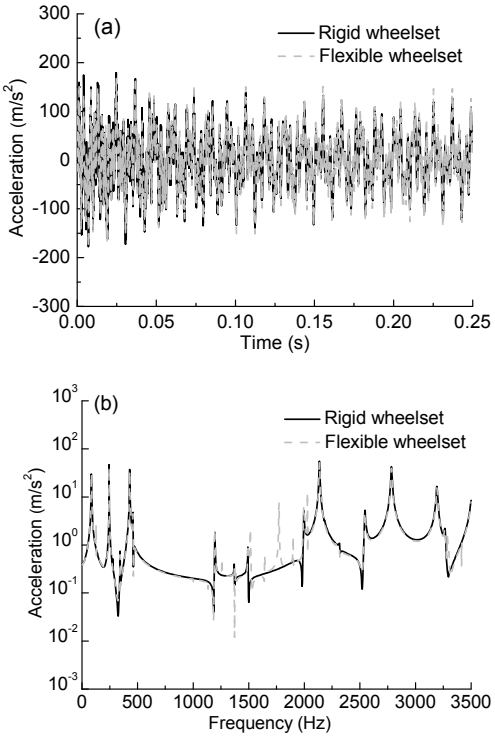

Fig. 5 Acceleration of rigid wheelset and flexible wheelset on tread: (a) time domain; (b) frequency domain

Fig. 6 shows the vertical acceleration of tread and lateral acceleration of tyre and web for a flexible wheelset. It is found that the acceleration of tread is excited at the frequencies of the radial modes, and the accelerations of tyre and web are significantly excited at the frequencies of the axial modes. These vibrations at high frequencies make the main contribution to wheel sound radiation.

Fig. 7 shows the sound pressure levels (SPLs) of rigid wheelset and a flexible wheelset at the point at a distance of 7.5 m from the middle of the track and at a height of 1.2 m from the railhead.

It can be seen in Fig. 7 that the noise components in mid-frequency and high-frequency ranges can be clearly characterized by using the present flexible wheelset mode as the wheel-rail contact force fluctuates in high frequency due to wheelset flexibility and the non-linear wheel-rail contact relationship. Some modes of wheelsets are excited by wheel-rail contact force at high frequencies and the peaks of these modes make a contribution to the total SPL of the wheelset. The total SPL obtained by the flexible wheelset model is 2.2 dB bigger than that of the rigid wheelset model. It means that the SPL will be

underestimated when the rigid wheelset model is used in predicting wheel-rail noise.

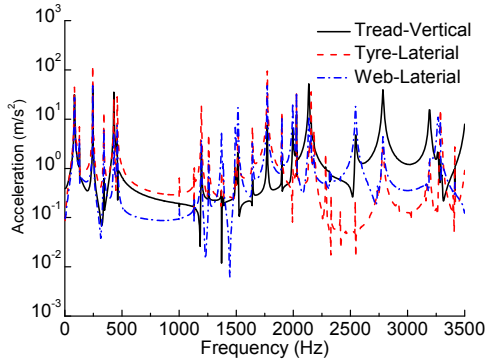

Fig. 6 Acceleration of a flexible wheelset in different locations

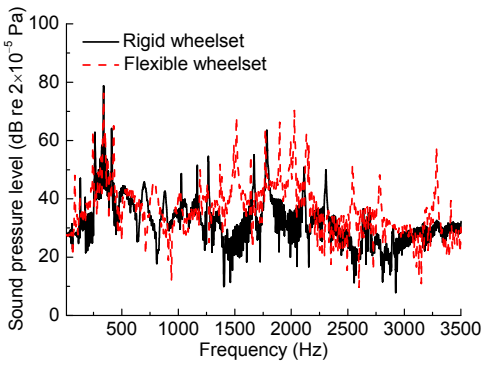

Fig. 7 Sound pressure level of rigid wheelset and flexible wheelset

4.3 Effect of rail corrugation on wheel-rail noise

Fig. 8 shows the effect of rail corrugation with wavelengths of 40–300 mm on wheel-rail noise using the flexible wheelset model at the point with distance of 7.5 m from the middle of the track and at a height of 1.2 m above the rail head. The amplitude of the corrugation is 0.02 mm. The speed is 300 km/h. The frequency range of 277–2083 Hz corresponds to the investigated passing frequency range of the corrugation.

Fig. 8 shows that the wheel-rail noise level decreases with the increase of the corrugation wavelength (40–300 mm) on the general trend. The local peaks of wheel-rail noise appear at a corrugation with wavelength of 250 mm. The peak at 250 mm corresponds to the wheelset modes of 327 Hz and 341 Hz, and the track mode of 331 Hz, which are simultaneously excited. The wheelset mode shapes of 327 Hz and 341 Hz are wheel web 'breathing' deformation in the same direction and the opposite direction without axle bending. The track mode shape of 331 Hz is rail deformation with high-order lateral bending.

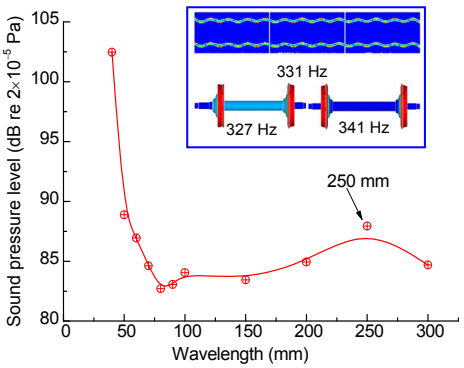

Fig. 8 Effect of rail corrugation on wheel-rail noise

5 Conclusions

In this paper, a numerical model of wheel-rail noise in the time-domain is developed based on vehicle-track coupling dynamics and considering flexible wheelsets and track, and the transient FE-BE wheel-rail noise prediction method. This time-domain model of wheel-rail noise can characterize noise components up to 5 kHz, and the present analysis frequency in this paper is up to 3.5 kHz. By using this model, the wheel-rail normal forces and the vibration and sound of rigid and flexible wheelset are analyzed. The effect of rail corrugation on wheel-rail noise is also calculated. The following conclusions can be drawn:

1. The fluctuation of the wheel-rail contact force considering the effect of wheelset flexibility is similar to that with a rigid wheelset at low frequencies. The main difference occurs at higher frequencies. The wheel-rail contact forces considering wheelset flexibility are lower when wavelength roughness excites a natural frequency of the wheelset, and higher when wavelength roughness excites an anti-resonance frequency. The wheel-rail contact force fluctuates at high frequency due to wheelset flexibility and wheel-rail nonlinear contact relationship.

2. The vibration and sound of flexible wheelsets are similar to those of rigid wheelsets below 500 Hz. The vibration and sound in the mid-frequency and

high-frequency ranges have more peaks and valleys. Moreover, the SPL can be underestimated when using the rigid wheelset model in predicting wheel-rail noise.

3. Wheel-rail noise decreases with the increase of the corrugation wavelength (40–300 mm) on the general trend. The peaks of wheel- rail noise appear at the corrugation wavelengths, where the wheelset modes are sensitive and excited.

In future work, it will be necessary to study the effect of wheelset rotation and flexibility together on wheel-rail noise in the time domain, especially for high-speed trains.

References

Baeza, L., Fayos, J., Roda, A., *et al*., 2008. High frequency railway vehicle-track dynamics through flexible rotating wheelsets. *Vehicle System Dynamics*, **46**(7):647-662. http://dx.doi.org/10.1080/00423110701656148

Baeza, L., Vila, P., Xie, G., *et al*., 2011. Prediction of rail corrugation using a rotating flexible wheelset coupled with a flexible track model and a non-Hertzian/ non-steady contact model. *Journal of Sound and Vibration*, **330**(18-19):4493-4507. http://dx.doi.org/10.1016/j.jsv.2011.03.032

Chaar, N., 2007. Wheelset Structural Flexibility and Track Flexibility in Vehicle/Track Dynamic Interaction. PhD Thesis, Kungliga Tekniska Högskolan, Stockholm, Sweden.

Chen, G., Zhai, W.M., 2004. A new wheel-rail spatially dynamic coupling model and its verification. *Vehicle System Dynamics*, **41**(4):301-322. http://dx.doi.org/10.1080/00423110412331315178

Delavaud, V., Chaigne, A., Poisson, F., 2010. Rolling noise simulation: a new approach in time domain. Proceedings in 10th International Workshop on Railway Noise.

Fang, R., Xiao, X.B., Fang, J.Y., *et al*., 2011. Influence of track structure parameters on acoustic radiation. *Journal of the China Railway Society*, **33**(5):78-84 (in Chinese).

Han, J., Zhao, G.T., Xiao, X.B., *et al*., 2015. Effect of softening of cement asphalt mortar on vehicle operation safety and track dynamics. *Journal of Zhejiang University-SCIENCE A (Applied Physics & Engineering)*, **16**(12): 976-986. http://dx.doi.org/10.1631/jzus.A1500080

Handoko, Y., Dhanasekar, M., 2006. An inertial reference frame method for the simulation of the effect of longitudinal force to the dynamics of railway wheelsets. *Nonlinear Dynamics*, **45**(3-4):399-425. http://dx.doi.org/10.1007/s11071-005-9016-6

Jin, X.S., 2014. Key problems faced in high-speed train operation. *Journal of Zhejiang University-SCIENCE A (Applied Physics & Engineering)*, **15**(12):936-945. http://dx.doi.org/10.1631/jzus.A1400338

Jin, X.S., Wen, Z.F., 2008. Effect of discrete track support by sleepers on rail corrugation at a curved track. *Journal of Sound and Vibration*, **315**(1-2):279-300. http://dx.doi.org/10.1016/j.jsv.2008.01.057

Ling, L., Han, J., Xiao, X.B., *et al*., 2015. Dynamic behavior of an embedded rail track coupled with a tram vehicle. *Journal of Vibration and Control*, **23**(14):2355-2372. http://dx.doi.org/10.1177/1077546315616521

Ma, X.T., 2007. Investigation on Prediction and Control of Railway Wheel-rail Rolling Noise. PhD Thesis, Beijing Jiaotong University, Beijing, China (in Chinese).

Meinders, T., 1998. Modeling of a railway wheelset as a rotating elastic multibody system. *Machine Dynamic Problems*, **20**:209-219. https://www.infona.pl/resource/bwmeta1.element.baztech-article-BWA1-0001-0369

Popp, K., Kruse, H., Kaiser, I., 1999. Vehicle/Track dynamics in the mid-frequency range. *Vehicle System Dynamics*, **31**(5-6):423-463. http://dx.doi.org/10.1076/vesd.31.5.423.8363

Popp, K., Kaiser, I., Kruse, H., 2003. System dynamics of railway vehicles and track. *Archive of Applied Mechanics*, **72**(11):949-961. http://dx.doi.org/10.1007/s00419-002-0261-6

Remington, P.J., 1987. Wheel-rail squeal and impact noise: What do we know? What don't we know? What do we go from here? *Journal of Sound and Vibration*, **116**(2): 339-353. http://dx.doi.org/10.1016/S0022-460X(87)81306-8

Remington, P.J., 1988. Wheel-rail rolling noise: What do we know? What don't we know? What do we go from here? *Journal of Sound and Vibration*, **120**(2):203-226. http://dx.doi.org/10.1016/0022-460X(88)90430-0

Shen, Z.Y., Hedrick, J.K., Elkins, J.A., 1983. A comparison of alternative creep-force models for rail vehicle dynamic analysis. *Vehicle System Dynamics*, **12**(1-3):79-83. http://dx.doi.org/10.1080/00423118308968725

Szolc, T., 1998a. Medium frequency dynamic investigation of the railway wheelset–track system using a discrete–continuous model. *Archive of Applied Mechanics*, **68**(1): 30-45. http://dx.doi.org/10.1007/s004190050144

Szolc, T., 1998b. Simulation of bending-torsional-lateral vibrations of the railway wheelset–track system in the medium frequency range. *Vehicle System Dynamics*, **30**(6): 473-508. http://dx.doi.org/10.1080/00423119808969462

Thompson, D.J., 1993a. Wheel-rail noise generation, Part I: introduction and interaction model. *Journal of Sound and Vibration*, **161**(3):387-400. http://dx.doi.org/10.1006/jsvi.1993.1082

Thompson, D.J., 1993b. Wheel-rail noise generation, Part II: wheel vibration. *Journal of Sound and Vibration*, **161**(3): 401-420. http://dx.doi.org/10.1006/jsvi.1993.1083

Thompson, D.J., 1993c. Wheel-rail noise generation, Part III: rail vibration. *Journal of Sound and Vibration*, **161**(3): 421-446.
http://dx.doi.org/10.1006/jsvi.1993.1084

Thompson, D.J., 1993d. Wheel-rail noise generation, Part IV: contact zone and results. *Journal of Sound and Vibration*, **161**(3):447-466.
http://dx.doi.org/10.1006/jsvi.1993.1085

Thompson, D.J., 1993e. Wheel-rail noise generation, Part V: inclusion of wheel rotation. *Journal of Sound and Vibration*, **161**(3):467-482.
http://dx.doi.org/10.1006/jsvi.1993.1086

Thompson, D.J., 2009. Railway Noise and Vibration: Mechanisms, Modelling, and Means of Control. Elsevier, Amsterdam, the Netherlands.

Thompson, D.J., Hemsworth, B., Vincent, N., 1996. Experimental validation of the TWINS prediction program for rolling noise, Part I: description of the model and method. *Journal of Sound and Vibration*, **193**(1):123-135.
http://dx.doi.org/10.1006/jsvi.1996.0252

Wu, T.X., Thompson, D.J., 2002. A hybrid model for the noise generation due to railway wheel flats. *Journal of Sound and Vibration*, **251**(1):115-139.
http://dx.doi.org/10.1006/jsvi.2001.3980

Xiao, X.B., Jin, X.S., Deng, Y.Q., *et al.*, 2008. Effect of curved track support failure on vehicle derailment. *Vehicle System Dynamics*, **46**(11):1029-1059.
http://dx.doi.org/10.1080/00423110701689602

Xiao, X.B., Ling, L., Xiong, J.Y., *et al.*, 2014. Study on the safety of operating high-speed railway vehicles subjected to crosswinds. *Journal of Zhejiang University-SCIENCE A (Applied Physics & Engineering)*, **15**(9):694-710.
http://dx.doi.org/10.1631/jzus.A1400062

Zhai, W.M., 1996. Two simple fast integration methods for large-scale dynamic problems in engineering. *International Journal for Numerical Methods in Engineering*, **39**(24):4199-4214.
http://dx.doi.org/10.1002/(SICI)1097-0207(19961230)39:24<4199::AID-NME39>3.3.CO;2-P

Zhang, Z., Dhanasekar, M., 2012. Dynamics of railway wagons subjected to braking torques on defective tracks. *Vehicle System Dynamics*, **50**(1):109-131.
http://dx.doi.org/10.1080/00423114.2011.571265

Zhong, S.Q., Xiong, J.Y., Xiao, X.B., *et al.*, 2014. Effect of the first two wheelset bending modes on wheel-rail contact behavior. *Journal of Zhejiang University-SCIENCE A (Applied Physics & Engineering)*, **15**(12):984-1001.
http://dx.doi.org/10.1631/jzus.A1400199

Zhong, S.Q., Xiao, X.B., Wen, Z.F., *et al.*, 2015. Effect of rotating flexible wheelset on wheel-rail rolling contact at high speed. Proceedings in 10th International Conference on Contact Mechanics.

Zhong, S.Q., Xiao, X.B., Wen, Z.F., *et al.*, 2016. Effect of wheelset flexibility on wheel-rail contact behavior and a specific coupling of wheel-rail contact to the flexible wheelset. *Acta Mechanica Sinica*, **32**(2):252-264.
http://dx.doi.org/10.1007/s10409-015-0441-6

中文概要

题　目：高速列车时域轮轨噪声预测模型及分析

目　的：建立高速列车时域轮轨噪声预测模型，考虑轮对柔性对轮轨噪声的影响，预测高速列车轮轨噪声的时域特性和频域特性，为高速轮轨时域噪声预测的学术研究和工程应用提供重要参考。

创新点：基于考虑轮对柔性的刚柔耦合车辆-轨道耦合动力学以及混合有限元-边界元方法，建立高速轮轨噪声时域模型。其中将柔性轮对的时域建模与轮轨噪声预测相结合是本文主要创新点。

方　法：1. 通过考虑柔性轮对的车辆-轨道刚柔耦合动力学模型（图 1）获得轮轨力，然后基于时域有限元-边界元方法（图 3），计算轮轨振动与噪声的时域结果，进而通过傅里叶变换得到频域结果。

结　论：1. 考虑轮对柔性与否，对低频轮轨力的影响较小。其主要差别体现在中高频范围，具体表现为：考虑轮对柔性后，当粗糙度波长与轮对固有频率重合时，轮轨力会降低；当粗糙度波长与轮对反共振峰重合时，轮轨力会提高；此外，因为考虑了轮对柔性以及接触的非线性，高频轮轨力的波动比考虑刚性轮对的轮轨力更为明显。2. 在 500 Hz 以下，考虑柔性轮对和刚性轮对得到的轮对振动和噪声差别不大，而在 500 Hz 以上的中高频范围内，振动噪声会出现更多的峰值和谷值；在中高频范围内，使用刚性轮对会低估轮轨噪声的水平。3. 轮轨噪声在总体趋势上随着波磨波长的增加而降低；在某些敏感波长对应的频率处，轮对或轨道的模态会被激发，使得轮轨噪声出现局部峰值。

关键词：振动声辐射；轮轨相互作用；车辆轨道耦合动力学；刚性轮对；柔性轮对；高速列车